Terahertz Active Direct Detection Imagers*

E. N. Grossman, A. Luukanen, A.J. Miller
Quantum Electrical Metrology Division, National Institute of Standards and Technology, Boulder, CO

ABSTRACT

We discuss several tradeoffs presented in the design of active imaging systems for the 100 to 1000 GHz frequency range, describe how we have addressed them in the design of a scanning, 95 GHz, bolometer-based imager for concealed weapons detection that is nearing completion, and describe how the system architecture can be modified to scale the operating frequency to the 650 GHz atmospheric window.

Keywords: Array, bolometer, concealed weapons, imaging, millimeter-wave, terahertz

1. INTRODUCTION

Considerable interest has developed recently in terahertz frequency imaging for applications in homeland security and defense[1]. While some applications are suitable for techniques such as time-domain spectroscopy, which are best adapted for small targets at close range, we focus here on systems operating with substantial standoff distances (> 1 m) and substantial fields-of-view (> 1 m diameter). Much of the recent interest in terahertz imaging derives from the substantial prior work on mm-wave imagers. For several years we have worked to develop an active mm-wave imaging system, described in the prior years of this conference[2], that is based on focal plane arrays (FPA's) of uncooled antenna-coupled microbolometers, and is optimized for simplicity and low cost. Its intended application is detection of weapons (metallic and non-metallic) concealed beneath clothing (CWD=concealed weapons detection). Last year we described the design and fabrication of a 120-element staring FPA, and some preliminary data using that FPA embedded in an active, pulsed imaging system with three angle-diverse illuminators. Detailed performance data on that FPA, including uniformity, sensitivity and noise-equivalent power (NEP), and coupling efficiency, is presented elsewhere in this conference[3] . As with most mm-wave imagers reported to date, the main avenues for advancing the capability of that system are pixel count and sensitivity. As described in detail elsewhere in this conference[4], a substantial improvement in sensitivity (approx. a factor of 6) has been realized by converting the uncooled Nb bolometers into freestanding airbridges, reducing their thermal conductance and thus improving responsivity and NEP.

To address the issue of pixel count, we have opted to reconfigure the FPA as a 128-element linear array and to employ a mechanically scanned optical system to synthesize 128(detectors) x 300 (scanner positions) = 38 kilopixel images at a 30 Hz frame rate. It is important to realize that actively illuminated imaging systems favor scanned architectures over staring architectures from the point of view of sensitivity. In the 95 GHz system nearing completion, polarizing optics is used to diplex the transmit and receive beams; perfect tracking is ensured by using the same scanner and focusing optics for both beams. The configuration of this scanned mm-wave imager is described at length in §3 below. An important feature of this scanned system is that, like the antenna-coupled microbolometers themselves, it can be scaled to higher frequency operation in a straightforward way. Higher frequency operation enables greater spatial resolution within the same footprint, or a reduced footprint at a given spatial resolution, since the spatial resolution is diffraction-limited and the footprint is dominated by the aperture size. We describe in §2 below several general points about the system architecture which are relevant both for the mm-wave scanned system presently under construction and for our planned migration to higher frequency.

2. SYSTEM ARCHITECTURE: MIGRATION TO TERAHERTZ FREQUENCY

a. Sensitivity requires active illumination in many applications

The motivation for using active illumination in the first place is sensitivity. Detection and imaging of natural blackbody emission is much more challenging at mm-wavelengths than in the thermal IR because of the much smaller bandwidth available at mm-wavelength (10's of GHz versus several THz) and because of the need for diffraction-limited spatial resolution, which restricts the number of spatial modes $N = \frac{A\Omega}{\lambda^2}$ available to any detector to 2 (for dual-polarization pixels) as opposed to typically ~50 for IR FPA's (A is the area and Ω the angular subtense corresponding to each pixel, and λ the operating wavelength). The single-mode condition is enforced at mm-wavelengths through the use of antennas to couple the detector to free space. To be specific, note that for diffraction-limited operation, the available power from a blackbody at temperature T is simply kTΔν, where Δν is the pre-detection bandwidth and k Boltzmann's constant. Therefore, the signal to noise ratio S/N for coherent detection of the contrast transmitted through a medium of transmittance t, between a warm body at temperature T_{body} and the background, at temperature T_{sky}, that is reflected off a target of reflectance r_{target} is given by the Dicke equation as

$$\frac{S}{N} = \quad 12 \quad \frac{t r_{\text{target}} \left(T_{\text{sky}} - T_{\text{body}}\right)_K}{\left(T_{\text{noise}} / 480K\right)} \left(\frac{\Delta\nu}{1GHz}\right)^{1/2} \left(\frac{\Delta t}{1/30\,\text{sec}}\right)^{1/2}. \qquad \textbf{(1)}$$

Here T_{noise} is the noise temperature of the coherent detection, either a mm-wave amplifier (e.g InP MMIC) followed by a direct detector, or a heterodyne receiver. The integration time is normalized to a standard video frame rate of 30 Hz. The noise temperature of 480 K corresponds to 1 % of the quantum limited sensitivity and is near the current state of the art for off-the-shelf components. Similarly for direct detection, the signal-to-noise ratio may be expressed in terms of the detector's noise-equivalent power (NEP) via

$$\frac{S}{N} = \quad 0.24 \quad \frac{t r_{\text{target}} \left(T_{\text{sky}} - T_{\text{body}}\right)_K}{\left(\frac{NEP}{1\ pW / Hz^{1/2}}\right)} \left(\frac{\Delta\nu}{100\,GHz}\right) \left(\frac{\Delta t}{1/30\,\text{sec}}\right)^{1/2}. \qquad \textbf{(2)}$$

The difference in assumed bandwidths in equations (1) and (2) reflects the fact that broadband operation is much more difficult to achieve with coherent systems than with direct detectors. For outdoor operation, where the temperature contrast can exceed 100 K, the sensitivity issue is tractable, but indoors, where many CWD applications require operation, the sensitivity challenge for passive operation is daunting.

Clearly, coherent detection is considerably more sensitive, and for this reason, the most successful mm-wave imagers to date[5] have all employed InP-based MMIC amplifiers as the front-end receiver. This approach has two major drawbacks however: the MMIC's are high cost, and they cannot be scaled to operating frequencies above ~ 200 GHz. For both these reasons we have focused on other uncooled detector approaches, primarily bolometers. Passive imaging with either bolometers or diodes is very challenging. The 1 pW/Hz$^{1/2}$ NEP figure in eqn. (2) is actually slightly beyond the present state-of-the-art for both uncooled bolometers or diodes. Schottky and metal-insulator-metal (MIM) diodes require a DC bias in order to access the highly nonlinear regions of their current-voltage (I-V) characteristics, where significant rectification occurs. This DC bias introduces very substantial 1/f noise however, which is ordinarily many orders of magnitude above the fundamental shot noise at a 30 Hz video frequency. The heterostructure backward diode[6], a relative newcomer, is a true zero-bias detector on the other hand. Recent noise measurements on these devices indicate exceptional sensitivity, an electrical NEP of 4 pW/Hz$^{1/2}$. They show great promise for the future but are currently limited to mm-wave operation by parasitic capacitance.

As for bolometric detectors, Figure 1 summarizes their sensitivity performance as a function of a key engineering parameter, the conductance of the bolometer's thermal isolation structure, G_{leg}. Microbolometers are very well understood devices, partly due to the extensive work done in the IR and partly due to extensive work on cryogenic bolometers. Excellent reviews have been written recently by Kruse (fundamental limits)[7], Wood[8] (uncooled IR arrays) and Richards[9] (chiefly cryogenic bolometers). Microbolometers are subject to a limitation on NEP due to fundamental thermodynamic fluctuations (often referred to as "phonon noise"), given by

$NEP(phonon) = \sqrt{4kT^2G}$. The solid traces in Fig. 1 correspond to this limit. The thermal conductance includes parallel contributions from the deliberately engineered conductance, the conductance of the air separating the bolometer from thermal ground (if it is operated in air), and the radiative thermal conductance linking the bolometer with the scene (the last yields the flat plateau in NEP in the low G_{leg} limit). Since the radiative thermal conduction is centered in the thermal IR ($\lambda \sim 10$ μm) , where the 300 K background is peaked, it is largely unaffected by the existence of the mm-wave antenna and is simply proportional to the (thermally isolated) bolometer area. The "current IR' traces correspond to hypothetical microbolometers comprising a bolometer element similar to that in present uncooled IR FPA's, 50 x 50 μm^2 in area, separated by ~ 2.5 μm from the substrate, but coupled to a much larger mm-wave antenna. The shaded regions of the plot indicate the areas in which the bolometer time constant is fast enough to permit a video frame rate under the listed conditions. The much greater speed of the NIST microbridge bolometers, as well as their much lower radiatively limited NEP, arises from the much smaller size of the microbridges, compared to IR microbolometers. This speed enables scanned operation at interesting sensitivity levels, which would otherwise be impossible.

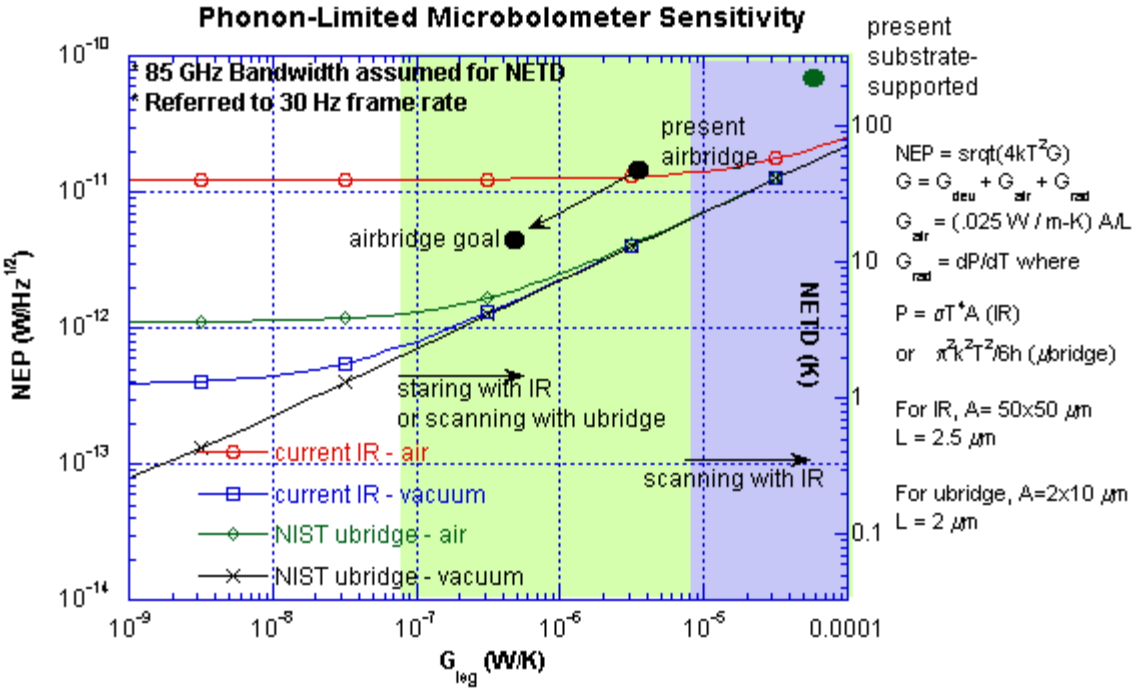

Fig. 1. Ultimate phonon-noise limited NEP for various uncooled bolometers, as a function of the (deliberately engineered) thermal conductance. Filled circles indicate measured electrical NEP for NIST Nb bolometers. The ranges of G for which microbridges and "IR-style" VOx bolometers (of the indicated dimensions) can support scanned operation are indicated by the shaded regions. 100 pixels are assumed to lie in the scan direction; the heat capacity of an IR bolometer is taken[8] as 3 nJ/K.

The phonon-limited NEP is rarely achieved in practice. Ordinarily, either Johnson noise, 1/f noise, or readout noise limits microbolometer sensitivity. In the case of the NIST microbolometer arrays, Johnson noise limits the sensitivity to about a factor of 3 worse than the phonon limit, a value which is not unusual for IR bolometers[8]. Thus, at values of NEP around 1 $pW/Hz^{1/2}$, bolometric detectors begin to run into fundamental limits, for the assumptions made in this analysis. Moreover, some allowance must be made in eqn. (2) for values of t and r_{target} that are significantly below unity. Therefore, even with an optimistic indoor temperature contrast of 10 K, the SNR for a passive bolometric imager cannot significantly exceed unity. Thus, the conclusion we draw from Fig. 1 and eqn. (2) is that passive imaging with bolometer arrays is simply not realistic without relaxing some of the assumptions in the above analysis.

One such relaxation that might be considered is increasing the bandwidth by operating at frequencies well above W-band. However, as shown in Fig. 2, $\Delta\nu$ cannot be increased much (factor of 2-3) beyond the quoted 100 GHz reference value without running into limits imposed by atmospheric transmission, at least in the type of standoff CWD applications we envision. The main advantage of higher frequency is not better sensitivity, but rather improved spatial resolution and/or reduced aperture size. Given the sensitivity challenge for purely passive operation, we therefore focus on active systems.

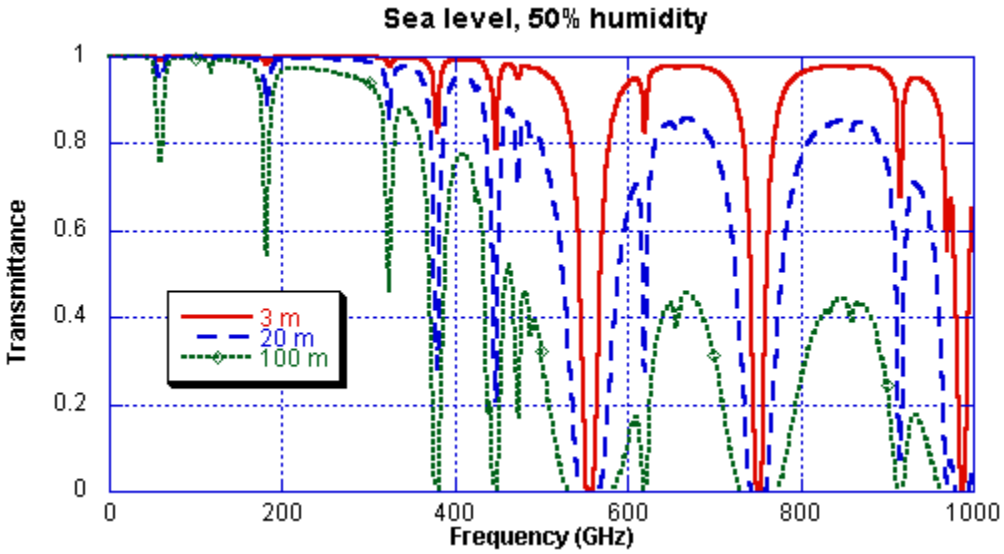

Fig. 2. Atmospheric transmission for sea-level horizontal one-way paths of 20 m, 50 m, and 100 m.

b. Active systems favor scanned rather than staring architectures.

It is a common intuition that staring arrays are always superior to scanned arrays, i.e. that a scanned array is only a regrettable compromise necessary to obtain high pixel count without the cost of higher detector count. The higher detector count of a staring array "must" provide a large advantage in sensitivity, and after all, CCD cameras, most uncooled IR imagers, and many other prototypical imagers are 2D staring arrays. For passive imaging, the superiority of staring arrays is perfectly true. For active systems however, it is a myth. Scanning systems are more sensitive if the illumination can be focused on just those pixels being observed at each instant of the scan. To be more specific, assume that the available illumination power and the total number of image pixels N_p are both held fixed. Furthermore, assume temporarily that the detector noise spectrum is white and that it dominates the signal-to-noise ratio (SNR) of the resulting images. The array has N_d physical detectors and N_p pixels in the image; for a staring array $N_d=N_p$ while for a scanned array $N_d/N_p = D$, the duty cycle (=1/number of pixels in the scan direction). The key is simply to examine how the signal-to-noise ratio scales with the duty cycle. In either array, the illumination power should be distributed evenly between all N_d detectors, so the available signal to each pixel scales as $1/N_d$. In a staring array, the full frame time is available for signal integration. In a scanning array, signal integration time is reduced by the duty cycle, $\tau \propto D$. Noise scales as $\tau^{-1/2}$, so signal-to-noise ratio scales as

$$SNR \propto N_d^{-1} D^{1/2} = N_p^{-1} D^{-1/2}.$$

The optimal strategy is therefore to use the lowest possible duty cycle, namely $1/N_p$, i.e. to have a "flying spot" architecture with a single detector and a rapidly scanned illumination beam, as in an SEM. If the noise is not white but is dominated by $1/f$ noise, then a similar argument[10] shows that SNR varies as D^{-1},and the advantage of scanning over staring is even greater than for white noise. Of course, there is the limitation that both the scanner and detectors must be fast enough to accommodate the higher pixel rate. Furthermore, the required optical performance of the scanner is demanding: transmit and receive beams must track one another on the target to within a diffraction spot. Aberrations or other optical imperfections not only degrade the spatial resolution by diffusing the receive beam, but also degrade the sensitivity by diffusing precious source power in the transmit beam over unobserved target pixels.

c. Pulsed operation is favored at 100 GHz, CW at high frequency

We are thus assuming a pixel rate of several kHz, (30 Hz frame rate x (N_p/N_d) in the scan direction). A new question arises which architecture is better, pulsed illumination and gated integration or modulated ("chopped") CW illumination and synchronous detection. We have discussed this before in connection with the mm-wave system[11]. The issue comes down to the performance of the illumination source: the figure of merit for the source is $P_{peak}D^{1/2}$ where D is the duty cycle. If the source is limited in average power $P_{avg}= P_{peak}D$ (for example by overheating), then pulsed operation (D << 1) is favored, while if it is limited by its peak power (for example by reverse breakdown in a diode) then CW operation (D = 1) is favored. For practical, low-cost systems, an all solid-state source is clearly required, and this brings the range of possibilities down to Gunn and Impatt oscillators at mm-wavelengths and diode-multiplied Gunn and Impatt oscillators at higher frequency. At mm-wavelength, pulsed Impatt oscillators with ~15 W and duty cycle of 0.5 % are commercially available (figure of merit ~ 1.1 W), whereas the highest power CW oscillator we are aware[12] of at W-band is 684 mW obtained with an experimental heterostructure barrier varactor diode. Thus, pulsed operation is favored at W-band. At high frequencies however, where the highest power solid-state source is likely to be a waveguide-coupled Schottky varactor, the opposite conclusion appears to be true. Table 1 (courtesy T. Crowe, VDI Inc.) details the performance of a waveguide-coupled Schottky varactor double, operating at 70 GHz output frequency, with a fixed peak power input of 8 W.

Duty cycle	Output power at 70 GHz (W)	Efficiency (%)	$P_{out}* D^{1/2}$ (W)
CW	1.4 W	17.5	1.4
10 %	2.0 W	25	0.63
4 %	2.7 W	33.8	0.54
2 %	3.1 W	38.8	0.44

Table 1. Performance of a waveguide-coupled Schottky varactor (courtesy T. Crowe, VDI Inc.).

d. Field-of-view limits; aberrations versus FPA real-estate

A system tradeoff exists in the design of microantenna arrays that manifests itself in the very basic questions of what the array pitch should be and what the preferred beamwidth of the microantenna pattern should be. (Since the antenna effective area varies inversely with the beamwidth, these two design choices are coupled.) The tradeoff arises because the microantenna array is necessarily coupled through some sort of mm-wave optics to the collecting aperture. The final f–number of this optics, i.e. the angular size of the exit aperture, must be matched to the beam of the microantenna elements to maximize the pattern –matching efficiency. That efficiency is simply a complex vector overlap integral between the antenna beam and the incident beam. The tradeoff is then:

- If the antenna pattern is broad and the optics fast, then the optics must be complex (many lens or mirror elements) in order to be diffraction-limited (rather than aberration-limited) over a large field-of-view. At the edge of the field-of-view (FOV) optical aberrations grow large and the coupling efficiency between each antenna and the optics degrades rapidly.
- On the other hand, if the antenna pattern is narrow and the optics slow, then the effective area of each antenna is large and their spacing on the focal plane must be increased. In this case, the field-of-view will be limited simply by the available real-estate in the focal plane. At mm-wavelengths, and even at THz wavelengths, this is a serious issue, as even fairly modest-sized arrays (say 100 pixels on a side) on pitches of order ~1 free-space wavelength are beyond the size that can be integrated monolithically, i.e.built on a single Si substrate. This also argues for a scanned system with an assembled (rather than monolithically integrated) FPA.
- Dielectric immersion optics only allows the spacing to be compressed in a certain limited sense. Simply bringing the beam in through the backside dielectric of a microantenna array reduces the wavelength by a factor of n (where n is the refractive index), but it increases the f-number of the beam by the same factor, so the diffraction limited spotsize is unchanged. In order to reduce the spotsize, some sort of integrated optics, such the fly's eye configuration, is required. Even this is not a complete solution however, since the spotsize is reduced but the spacing remains limited by the lenses. In other words, such an arrangement takes a hit in aperture efficiency by n (for each dimension, n^2 overall).

The issue is now fairly clear; patterns for purely planar antennas tend to be quite broad, i.e. low gain. On the other hand, although designing and using very fast (f/1 or less) optics to focus onto a single element is relatively

straightforward, a very complex (many element) lens would be required to form a high quality (i.e. diffraction limited) image over any significant field of view. Mm-wave optics are considerably less evolved than IR optics in general. Far fewer good lens materials exist (polyethylene is the material of choice for large mm-wave optics,) and the repertoire of existing designs is far smaller. As the number of lens (or mirror) elements increases, so does the loss. Polyethylene has a 4 % loss per surface just from dielectric mismatch, similar to optical glass, as well as significant bulk absorption, so the loss from a multi-element lens can be significant in the overall sensitivity budget.

The net effect of this tradeoff is to impose a limit on the **system** field-of-view. At one end of the tradeoff, the FOV is limited by optics, aberrations and loss, at the other end by real estate in the focal plane. For the 95 GHz system, we have opted for a rather slow optical feed and antenna pattern, choosing to ease the optics limitation and to mechanically assemble a very large FPA. The latter consists of 128 slot-ring antenna-coupled elements (identical to those used in the 120-element staring array[3], arranged in a line at 9.5 mm spacing. This is in fact a factor of two undersampled compared to the staring array, but, for a fixed number of detectors and readout channels, we have judged was it more important in the first version to cover the full field-of-view than to preserve ideal sampling.

3. SCANNING, 128X300 MM-WAVE IMAGING SYSTEM

As mentioned above, our approach for increasing pixel count to the 10^4 range is a mechanically scanned, 1-D linear array. Although our first implementation of this approach is at 95 GHz, migration to higher frequencies informs the entire system design. The use of microbolometers makes this migration possible. We here describe the specifications and design of the 95 GHz system. Most of the components are complete, but assembly of the system has not yet started, as of this writing.. The system is intended to operate as a portal, imaging a full human figure as a person steps into the 0.9 x 1.8 m field-of-view. The target distance, from the field-of-view to the entrance aperture, is 1.5 m. The entrance aperture diameter is 48 cm, yielding an f-number of 3.1 at the target, and a diffraction-limited spotsize of of $f\lambda$ = 1 cm. The pixel count is 128 (detectors) x 300 (scanner positions) = 38,400 pixels.

a) Scanner and lens design

The polyethylene entrance and exit lenses are identical separated doublets, each with four aspheric surfaces. A detailed ray trace (see fig. 4) indicates the resolution is diffraction limited (rather than aberration-limited) over the entire field-of view. A scale diagram of the scanned system layout is shown in Fig. 3. The operation is relatively straightforward. Linearly polarized power from the source is focused into a "virtual FPA", a 1-dimensional image matching the overall aspect ratio of the linear FPA, and then reflected off a properly oriented grid polarizer. The source and the real FPA are each linearly polarized and orthogonal to one another, the grid polarizer serving to diplex the transmit and receive beams. The transmit beam then reflects off the bending mirror and is transformed into an array of collimated beams (at angles corresponding to position in the virtual FPA) by the exit lens. The collimated beams are reflected off the conical scanner, a flat mirror rotating at the frame rate (i.e. 30 Hz) about an axis which lies at 45^o from the incident beam. The mirror surface is offset by several degrees from orthogonal to the rotation axis. The collimated beams directed toward the entrance lens therefore sweep out a conical surface, and then are focused onto the target by the entrance lens. Each focused beam traces out an elliptical path at the target. At the entrance lens, a quasi-optical quarter-waveplate transforms the transmit beams to circular polarization. Fig. 4 indicates the paths traced on the target by the beams corresponding to various detectors in the FPA. Note that the sampling on the focal plane is highly non-uniform, with "pile-up" of the traces at the edges of the field, and extensive crossing of tracks from different detectors. However, there is complete coverage of the full field-of-view. The redundancy in the coverage (i.e. the crossing of the tracks) is a significant advantage in image processing, enabling calibration of the relative detector gains ("flat-fielding" of the FPA) in real time. At the target, a fraction of the incident power is scattered back into the entrance lens, now with the opposite sense of circular polarization. It passes back along the same path through the system, but is now transmitted through the grid polarizer and focused onto the real FPA.

The chief advantage of this system is that at any given instant in the scan, the only area of the target being illuminated is the area which the scanner is focusing onto the FPA at the same instant. The source power is used only where it is needed, enabling fairly low levels of illumination to produce large signals even on relatively insensitive (compared to a MMIC amplifier) detectors. The transmit and receive beams track each other very well because they are each being scanned by the same optics.

b) Polarization-based transmit/receive diplexing

The most straightforward means of implementing the polarizing beamsplitter and the quarter-waveplate is as etched metallic patterns supported on low-loss circuitboard or kapton substrates. The pattern for the polarizer is simply an array of parallel wires, while quarter-waveplates can be realized with arrays of meandered wires[13], with "waffle-grid" patterns[14] consisting of alternating solid and dashed lines, or with arrays of capacitively loaded dipoles[15]. In each case, the grid presents a capacitive surface to one polarization and an inductive surface to the orthogonal one. Achievement of acceptable polarization purity (axial ratio) over a large angular field-of-view requires careful design. The waffle-grid pattern has been selected in our case for low-cost manufacturability.

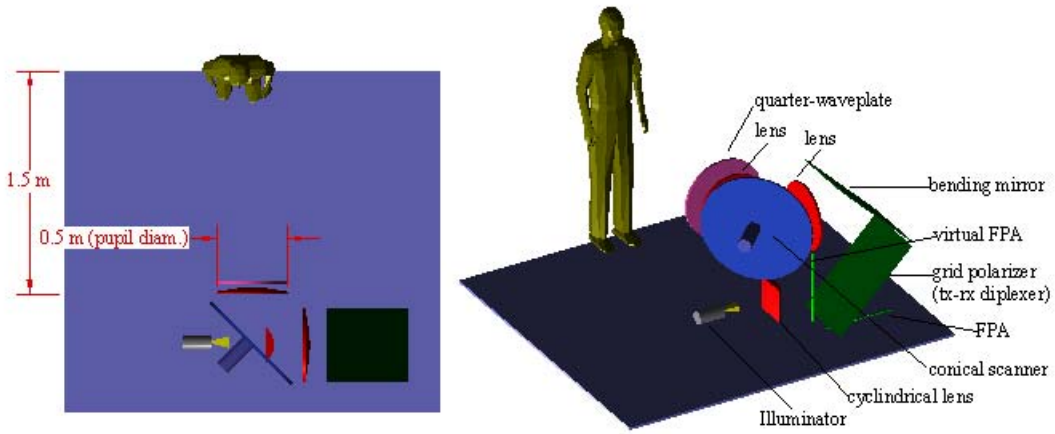

Fig. 3. Block diagram of active scanned mm-wave imaging system under construction

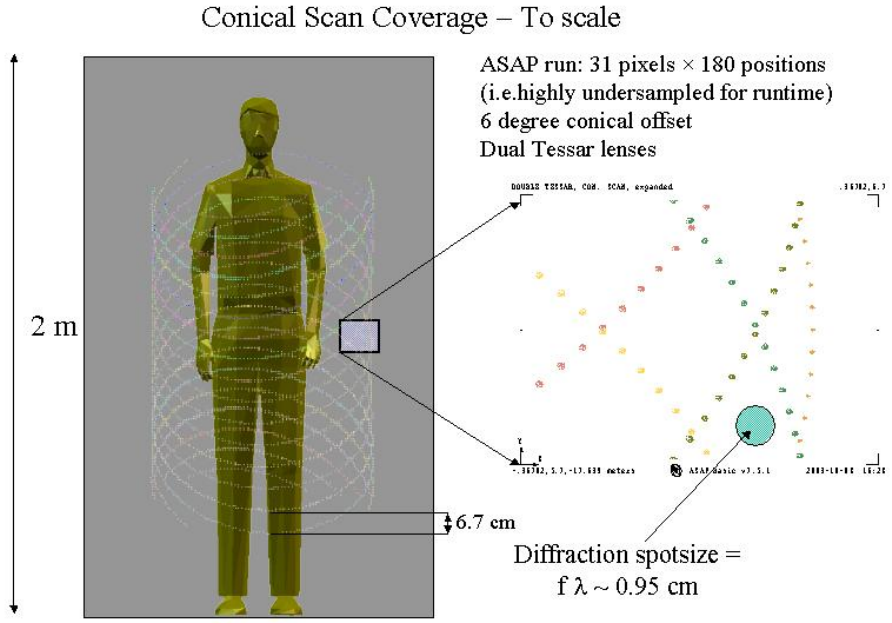

Fig. 4. Object plane sampling of scanned active system. Each spot in the tracks is an accurate individual spot diagram through the entrance and exit lenses (Tessar in this case). The number of detectors and scan positions has been reduced for clarity. The field-of-view, controlled by the size of the FPA and the angular offset in scanner is somewhat lower in this diagram than in the final design. Note the non-uniform object sampling.

e. Sensitivity estimates: 95 and 650 GHz

Besides the 95 GHz system currently under construction, we have performed a detailed sensitivity analysis of a version scaled for operation in the 650 GHz atmospheric window. The 650 GHz version will differ from the mmw version in certain ways (see table). It will be designed for a 2 m x 4 m field of view at a target distance of 5 m. It will have a substantially smaller footprint (by approx a factor of 2 in each dimension) because of a smaller aperture (25 vs. 50 cm diameter), while the lens performance is significantly less demanding because of the smaller angular field-of-view at 5 m range. The lenses, which in the mmw version are aspheric doublets optimized for low aberration, will be optimized for significantly lower thickness at 650 GHz, since the loss of polyethylene is significantly higher at the higher frequency, namely ~ 9 % / cm. As discussed above, the source for the 650 GHz system will be a waveguide-coupled Schottky varactor multiplier, operated CW. A power level of 3 mW for such a source seems likely in light of recent tests on similar units[16]. For the 650 GHz system, we have assumed use of our new Nb airbridge microbolometers[4], with a measured electrical NEP of ~ 15 pW/Hz$^{1/2}$, as opposed to the substrate-supported microbolometers[3] that are incorporated into the 95 GHz system. The most questionable part of any such sensitivity analysis is the assumption regarding target reflectance. As a baseline assumption, we have used a perfectly diffuse target reflectance. With these assumptions, a basic system sensitivity estimate is quite straightforward:

The power per pixel incident on the target is $P_i = \eta_s \frac{P_s}{N_d}$,

the geometric dilution factor for diffusely scattered light is $G = \frac{\Omega_{ap}}{2\pi} = \frac{d_{ap}^2}{8L^2}$,

the pixel dwell time for the scanning is $\tau = \tau_{frame} D$, so

the RMS uncertainty in the received power is $\sigma = NEP_e \left(2\tau_{frame} D\right)^{-1/2}$.

Here, P_s is the source power, η_s the efficiency of the source illumination (source reference plane to target), η_d the efficiency of the detection system (target to antenna terminals), L the range, d_{ap} the collecting aperture diameter, Ω_{ap} the solid angle subtended at the target by the collecting aperture, NEP_e the electrical NEP of the detector, and τ_{frame} the frame time = 1/30 s. If one assumes the target reflectance is perfectly diffuse, i.e. that all power incident on each pixel of the target is uniformly scattered over 2π srad, then one obtains for a baseline signal-to-noise ratio (1 frame)

$$SNR_{\text{base}} = \frac{P_s}{NEP_e}\left(\frac{\eta_s \eta_d d_{ap}^2}{8L^2}\right)\frac{\left(2\tau_{\text{frame}}\right)^{1/2}}{\left(N_p N_d\right)^{1/2}} \quad . \tag{3}$$

SNR is dominated by source power and detector NEP. The above relation is illustrated in Fig. 5, which displays SNR_{base} on a per-pixel, per frame basis as a function of range, for three assumptions about source power and detector NEP, which correspond to the 95 GHz system, the baseline 650 GHz system described above, and a hypothetical 650 GHz system with source power and NEP well beyond what is available today.

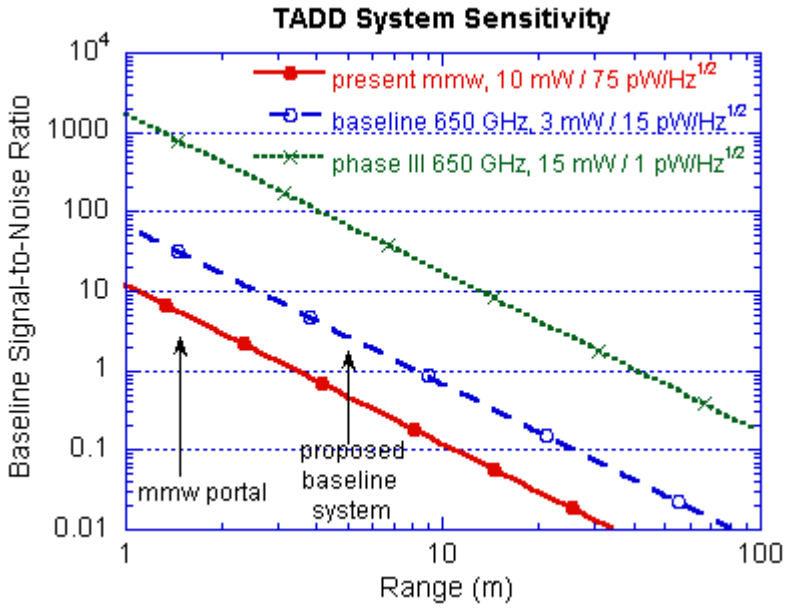

Fig. 5. Baseline signal-to-noise ratio as a function of range to target. Assumptions for the baseline and final TIFT systems are D_{ap} = 0.25 m, N_dx N_p = 128 × 300, η_s =0.5, η_d =0.25, and 30 Hz frame rate. For the mmw portal, D_{ap} = 0.5 m, η_s =0.25, η_d =0.1 are used.

Specification	Value	Specification	Value
Frequency	650 GHz	Pixel count	128 × 300
Range	5 m	Illumination power	3 mW
Aperture Size	25 cm	Illumination efficiency	25 %
Field-of-view	2 × 4 m (h × w)	Detection efficiency	50%
Frame Rate	30 Hz	NEP	5 pW/Hz$^{1/2}$
Spatial resolution	1 cm	S/N ratio (one 30 Hz frame)	3

Table 2. Baseline 650 GHz system specifications and performance

4. CONCLUSIONS

We have described the design of a new mechanically scanned 95 GHz imaging system based on a 1-D array of antenna-coupled Nb microbolometers. The microbolometers and the overall system design are both straightforwardly scalable to higher frequency, and we have also described a number of system issues relevant to such scaling. These include the need for active illumination in order to enable application for indoor CWD, the fact that active illumination favors scanning rather than staring architectures, so long as the illumination tracks the scanning of the detection (as it does in our design), the fact that pulsed operation is favored at low frequency while CW operation is favored at higher frequency, and the limits on field-of-view imposed by FPA area or by optical aberrations.

5. ACKNOWLEDGEMENTS

We are grateful to Kathleen Higgins and Nick Paulter of the Office of Law Enforcement Standards for originally starting this program, under National. Institute of Justice sponsorship. We are grateful to Tom Crowe of Virginia Diodes Inc. for use of unpublished data.

6. REFERENCES

[1] See these proceedings (SPIE vol. 5411) and those of related conferences, SPIE Proc. Vol 5410.
[2] E.N. Grossman and A. J. Miller, "Active Millimeter-wave Imaging for Concealed Weapons Detection", *Proc. SPIE,* **v. 4013**, pp. (2003)
[3] A. Luukanen, A. J. Miller, E. N. Grossman, "Active Video Rate Imaging with a Staring, 120-element, Microbolometer Array", these proceedings
[4] A.J. Miller, R.A.M. Luukanen, and E.N. Grossman, "Uncooled Nb Airbridge Microbolometers for MM-wave Imaging", these proceedings
[5] P. Moffa, L.at al., "Large-aperture Passive Millimeter-wave Pushbroom Camera", *Porc. SPIE*, **v.4373**, pp. 1-6 (2001), R. Appleby et al., "Mechanically Scanned Real-time Passive Millimeter-wave Imaging at 94 GHz", *Proc. SPIE,* **v. 5077**, pp. 1-6, (2003)
[6] P. Fay, J.N. Schulman, S. Thomas III, D.H. Chow, Y.K. Boegman, and K.S. Holabird, "High-performance Antimonide-base Heterostructure Backward Diodes of Millimeter-wave Detection", *IEEE Electron Device Lett.*, **v. 23(10)**, pp. 585-587, (2002), and J.N. Schulman and D.H. Chow, "Sb-Heterostructure Backward Diodes", *IEEE Electron Device Lett.*, **v. 21(7)**, pp. 353-355 (2000)
[7] P. W. Kruse, "Principles of Uncooled Infrared Focal plane Arrays", chap. 2 in *Uncooled Infrared Focal Plane Arrays",* ed. P. W. Kruse and D. D. Skatrud,, v. 47 of *Semiconductors and Semimetals*, Academic Press, 1997
[8] R. A. Wood, "Monoli,thic Silicon Microbolometer Arrays", chap. 3 *ibid.*
[9] P. A. Richards, "Bolometers for Infrared and Millimeter Waves", J. Appl. Phys., **76** (1), p.1-24, (1994)
[10] Allen, D.W., *Should the Classical Variance be Used as a Basic Measure in Standards Metrology ?* IEEE Trans. Instrumentation and Measurement, **IM-36**(2): p. 646-654 (1987).
[11] S. Nolen, J.A. Koch, N.G. Paulter, C.D. Reintsema, and E.N. Grossman, "Antenna-coupled Niobium Microbolometer for Millimeter-wave Imaging Arrays", *Proc. SPIE* **3795**, pp. 279-286
[12] J.B. Hacker, A.L. Sailer, B. Brar, G. Nagy, R. L. Pierson Jr., and J.A. Higgins, "A High-power W-band Quasi-optical Frequency Tripler", *IEEE Microwave Symposium Digest*, **v. MTT-S 3,** pp. 1859-1862 (2003)
[13] R-S. Chu and K-M. Lee, "Analytical model of a Multilayered Meander-line Polarizer Plate with normal and Oblique Plane-wave Incidence", *IEEE Trans. Ant.and Prop.* ,**AP-35 (6)**, pp. 652-661 (1987)
[14] K.M.K.H. Leong and W.A. Shiroma, "Waffle-grid Polarizer", *Electronics Lett.*, **v. 38(22)**, pp1360-1361 (2002)
[15] S. Hollung, W. Shiroma, M. Markovic, and Z.B. Popovic, "A Quasi-optical Isolator", *IEEE Microwave and Guided Wave Lett.*, **v. 6(5)**, pp. 205-206 (1996)
[16] T. Crowe, Virginia Diodes Inc., private communication